Adrenal Gland Imaging

16

Jessica T. Casey, Earl Y. Cheng,
and James S. Donaldson

Abbreviations

ACTH	Adrenocorticotropic hormone
AIDS	Acquired immunodeficiency syndrome
CAH	Congenital adrenal hyperplasia
CT	Computed tomography
DOPA	Dihydroxyphenylalanine
EBV	Epstein-Barr virus
FDG	Fluorodeoxyglucose
HVA	Homovanillic acid
INSS	International Neuroblastoma Staging System
MDP	Methylene diphosphonate
MEN	Multiple endocrine neoplasia
MIBG	Metaiodobenzylguanidine
MR	Magnetic resonance imaging
17-OHP	17-hydroxyprogesterone
PET	Positron emission tomography
US	Ultrasonography
VIP	Vasoactive intestinal peptide
VMA	Vanillylmandelic acid

J.T. Casey, MS, MD
Department of Urology,
Northwestern University Feinberg School of Medicine,
303 E Chicago Avenue, Tarry 16-703,
Chicago, IL 60611, USA
e-mail: jtcasey@fsm.northwestern.edu

E.Y. Cheng, MD (✉)
Division of Urology, Ann and Robert H. Lurie
Children's Hospital of Chicago,
Northwestern University Feinberg
School of Medicine, 225 E Chicago Avenue,
Chicago, IL 60611, USA
e-mail: echeng@luriechildrens.org

J.S. Donaldson, MD
Radiology, Department of Medical Imaging,
Ann and Robert H. Lurie Children's Hospital of Chicago,
Northwestern University Feinberg School of Medicine,
225 E Chicago Avenue, Chicago, IL 60611, USA
e-mail: jdonaldson@luriechildrens.org

Normal Anatomy, Physiology, and Embryology

The adrenal glands are paired retroperitoneal organs consisting of an outer cortex derived from the intermediate mesoderm of the urogenital ridge and an inner medulla derived from neural crest cells [1]. The crescent-shaped left adrenal gland is located anteromedially to the superior pole of the left kidney and lateral to the aorta [1]. The triangular right adrenal gland is located on the superior pole of the right kidney slightly behind the inferior vena cava [1]. Three separate arteries supply the adrenal glands: superior adrenal artery (originates from the inferior phrenic artery), middle adrenal artery (originates from the aorta at the level of the celiac plexus), and inferior adrenal artery (originates from the main renal artery) [1]. One adrenal vein drains each adrenal gland: the right adrenal vein drains directly into the inferior vena cava, and the left adrenal vein drains into the left renal vein; however, variants in adrenal vein drainage have been described [1, 2].

The cortex of the adrenal gland is composed of three zones: the outermost zona glomerulosa

L.S. Palmer, J.S. Palmer (eds.), *Pediatric and Adolescent Urologic Imaging*,
DOI 10.1007/978-1-4614-8654-1_16, © Springer Science+Business Media New York 2014

which produces mineralocorticoids (primarily aldosterone), the middle zona fasciculata which produces glucocorticoids (such as cortisol), and the innermost zona reticularis which produces sex steroids (such as adrenal androgens and estrogens) [3]. Hormone synthesis from the adrenal cortex is controlled by the hypothalamic-pituitary-adrenal axis via corticotrophin-releasing hormone (from the hypothalamus) and adrenocorticotropic hormone (ACTH, from the pituitary) [3]. The adrenal medulla, which encompasses less than 10 % of adrenal mass, releases catecholamines (epinephrine, norepinephrine, and dopamine) as part of the autonomic nervous system [4].

At birth, the fetal adrenal gland is twice the weight of an adult adrenal gland and about one-third the size of the kidney due to the presence of the fetal adrenal cortex, which initially composes 80 % of the adrenal gland mass [3, 5]. The adrenal gland's large size at birth makes them easily visualized by ultrasonography (US) during the neonatal period [1, 3]. Atrophy of the fetal cortex begins after birth and is resorbed completely by 12 months of age [3, 6]. During this time, the zona glomerulosa and fasciculata of the adult adrenal cortex begin to develop; however, the zona reticularis does not completely differentiate until 3 years of age [7, 8].

General Concepts of Normal Adrenal Imaging

As early as the second trimester of pregnancy, the adrenal glands can be visualized by antenatal US. Given the relatively large size of the neonatal adrenal gland due to the presence of fetal adrenal cortex, US can easily visualize the adrenal glands during the neonatal period [1]. After the fetal cortex has involuted, US cannot reliably discern anatomic details of the adrenal glands. Thus, computed tomography (CT) and magnetic resonance imaging (MR) are best employed for imaging the adrenal glands in children and older infants [1].

On US, the normal appearance of the adrenal gland is two separate zones of echogenicity: a core consisting of a thin, central hyperechoic stripe (representing the central veins, the connective tissue, and the relatively small neonatal medulla) and a surrounding rim of thicker hypoechoic tissue (representing the fetal and peripheral adult adrenal cortex) (Fig. 16.1) [5]. In some neonates, the thin, central hyperechoic core is replaced by a broader band of echogenicity, likely representing congested sinusoids resulting from hemorrhagic necrosis of the involuting fetal adrenal cortex in addition to the neonatal medulla and central veins [5]. The surface of a normal neonatal adrenal gland is smooth to slightly

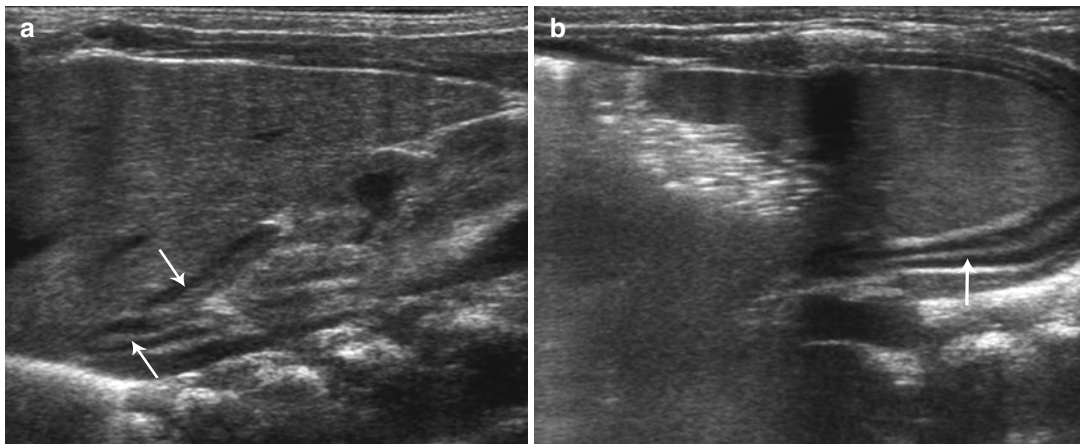

Fig. 16.1 Normal infant adrenal gland – US. Longitudinal ultrasound image of the right adrenal gland (**a**) and transverse ultrasound image of the left adrenal gland (**b**) in a 2-month-old girl illustrate the normal appearance (*arrows*) with hypoechoic adrenal cortex surrounding the central echogenic adrenal medulla creating an "Oreo cookie" appearance

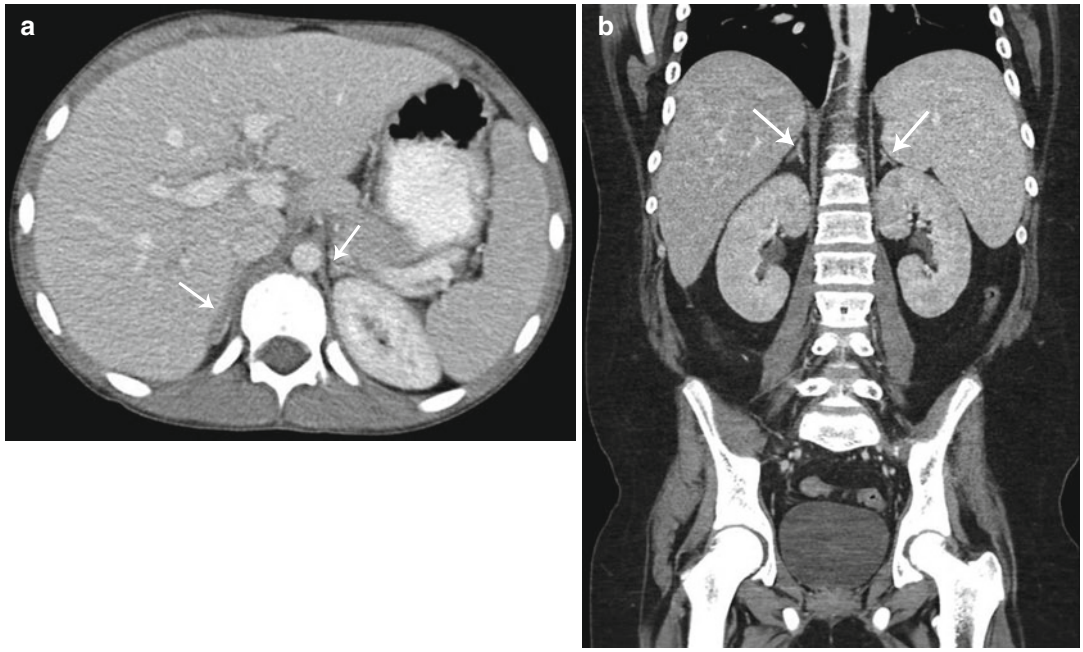

Fig. 16.2 Normal adrenal gland – CT. Axial contrast-enhanced CT image in a 12-year-old girl (**a**) and coronal contrast-enhanced CT image in a 14-year-old boy (**b**) show normal size and appearance of the adrenal glands (*arrows*) which are isodense to the liver

undulating, without nodular protuberances [3, 5]. In normal adrenal glands, limbs should be uniform in length, and their width should be less than 4 mm [5, 9]. The adult appearance of the adrenal gland is formed between 1 and 3 years of age, and they may be seen as very thin, linear, hypoechoic structures isoechoic to the liver [10].

The adrenal glands can be visualized anteromedial to the upper pole of the ipsilateral kidney at all ages on both CT and MR [1]. The right adrenal gland lies medial to the right lobe of the liver, lateral to the right crus of the diaphragm, and posterior to the inferior vena cava [1]. The left adrenal gland lies medial to the spleen, lateral to the aorta and left crus of the diaphragm, and posterior to the pancreatic tail and stomach [1]. To estimate normal adrenal size, the adrenal glands should be thinner than the adjacent diaphragmatic crura on axial images [1]. CT and MR can similarly demonstrate detailed information on adrenal anatomy; though, in determining the modality of choice, their respective risks and benefits should be considered (e.g., radiation exposure from CT and the risk of sedation during MR). On CT, the adrenal gland's soft tissue attenuation is similar to the liver (Fig. 16.2) [11]. For MR, on spin-echo T1-weighted images, adrenal glands have intermediate signal intensity (less than fat and similar to the liver); on T2-weighted and fat-suppressed images, adrenal glands are much brighter than fat and slightly brighter than the liver (Fig. 16.3) [11].

Anomalies of Shape and Position of the Adrenal Gland

As adrenal development and renal development are separate processes, adrenal glands will develop in their normal position within the retroperitoneum despite ipsilateral renal agenesis, malrotation, or ectopia [12]. However, in these cases, they are often flattened or discoid in shape, as well as slightly longer and thicker (referred to as a "straight adrenal gland") (Fig. 16.4) [5, 6, 11, 13]. This straight adrenal gland is not seen after nephrectomy or acquired renal atrophy [5].

Anomalies of the adrenal glands are exceedingly rare. The two most common fusion anomalies are

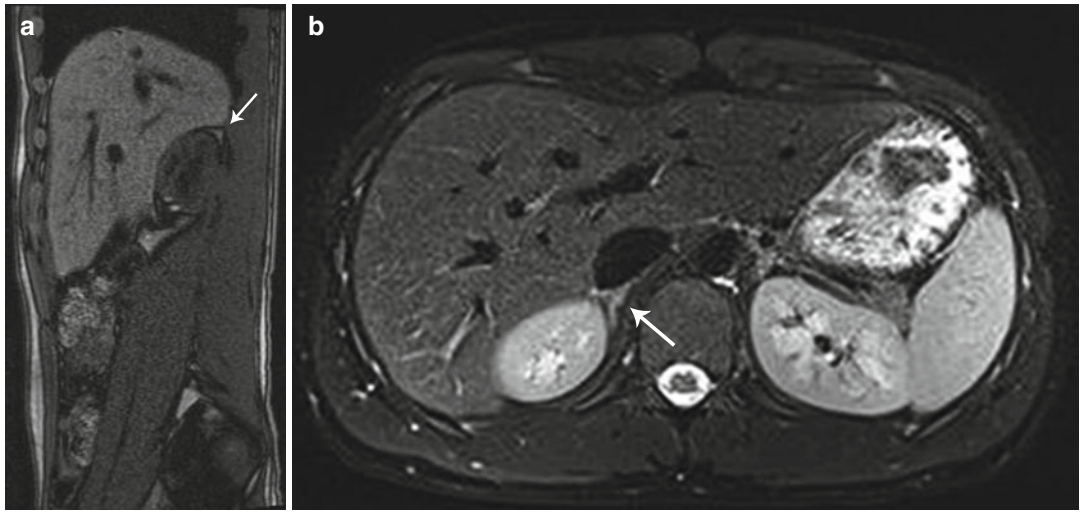

Fig. 16.3 Normal adrenal gland – MR. MR images in a 13-year-old boy reveal normal adrenal gland. On sagittal T1 images (**a**) the adrenal gland (*arrows*) is intermediate signal intensity similar to the liver. On axial T2 fat-suppressed images (**b**) the right adrenal gland (*arrow*) is intermediate signal intensity and brighter than the adjacent liver

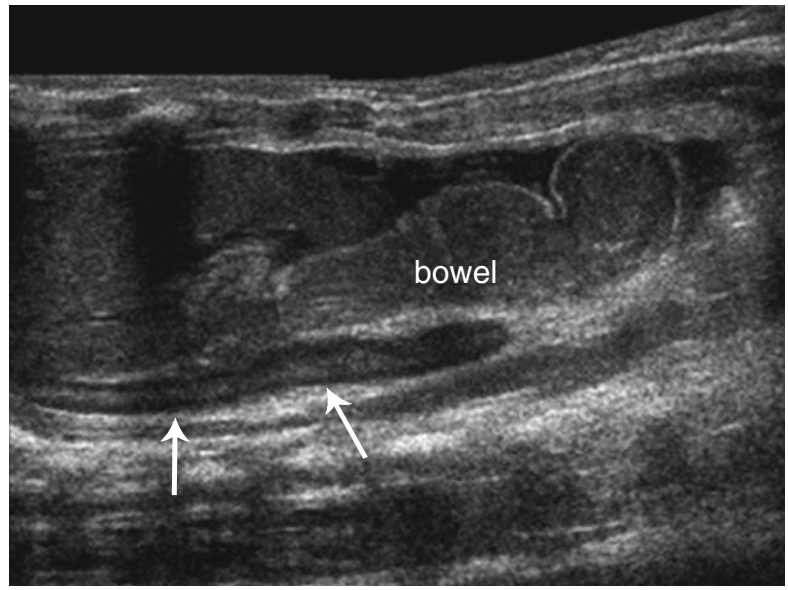

Fig. 16.4 Renal agenesis. Longitudinal ultrasound image of the left upper quadrant in a neonate with left renal agenesis. Bowel loops fill the left renal fossa with a straight, discoid left adrenal gland (*arrows*) seen

the circumrenal adrenal and the horseshoe adrenal [3, 14]. In the circumrenal adrenal, the fused limbs fuse around the upper pole of the ipsilateral kidney [3, 14]. Horseshoe adrenal describes fusion of the right and left adrenal glands in the midline anterior to the spine and posterior to the aorta [3, 14]. Horseshoe adrenals are often associated with renal anomalies (horseshoe kidney, renal agenesis), central nervous system anomalies such as neural tube defects, and asplenia with visceral heterotaxy [3, 14]. The isthmus of the horseshoe adrenal usually passes posterior to the aorta, but in association with asplenia the isthmus passes anterior [14].

Adrenal rests, or accessory adrenal glands, are mainly composed of cortical tissue, with the occasional presence of medullary tissue. They can be found anywhere along the path of gonadal descent in the retroperitoneum. Most commonly they are located near the celiac plexus, but can also be seen along the course of the gonadal veins and within the broad ligament, ovary, inguinal canal, testes, and epididymis [3]. Adrenal rests

typically atrophy with time; therefore, although they can be found in up to 50 % of neonates, they are found in only 1 % of adults [7]. Males with congenital adrenal hyperplasia have a high prevalence of persistent adrenal rests in the testes [15].

Anomalies of Size of the Adrenal Gland

Congenital Adrenal Hyperplasia

Congenital adrenal hyperplasia (CAH) is collection of autosomal recessive disorders characterized by low cortisol production, potential aldosterone deficiency, and androgen excess due to an enzymatic defect in the cholesterol-steroid biosynthesis pathway [5]. Over 95 % of cases are due to a deficiency in the enzyme 21-hydroxylase [5]. Androgen excess leads to virilized genitalia in female infants and early virilization in male infants [11]. In the most severe form, concomitant aldosterone deficiency leads a salt-losing crisis in either sex during the newborn period [5]. Diagnosis can be made by a very high concentration of 17-hydroxyprogesterone (17-OHP) after three days of life [16].

Most neonates with CAH have enlargement of the adrenal glands with a width measurement of >4 mm and a length measurement of >20 mm [17]. Additional signs which may be seen on US include a cerebriform appearance of the surface of the adrenal gland and a stippled central adrenal echogenicity [18, 19]. In a series by Al-Alwan et al., US in the immediate neonatal period had a sensitivity of 92 % and a specificity of 100 % for the diagnosis of CAH and may be employed before conclusive 17-OHP levels are available [18]. Diagnosis of CAH can be made by the demonstration of two of three sonographic signs: (1) adrenal limb width of >4 mm, (2) cerebriform or crenated appearance of the surface of the adrenal gland, and (3) replacement of the central hyperechoic stripe with a diffusely stippled pattern of echogenicity or a diffuse thickened band of echogenicity (Fig. 16.5) [18].

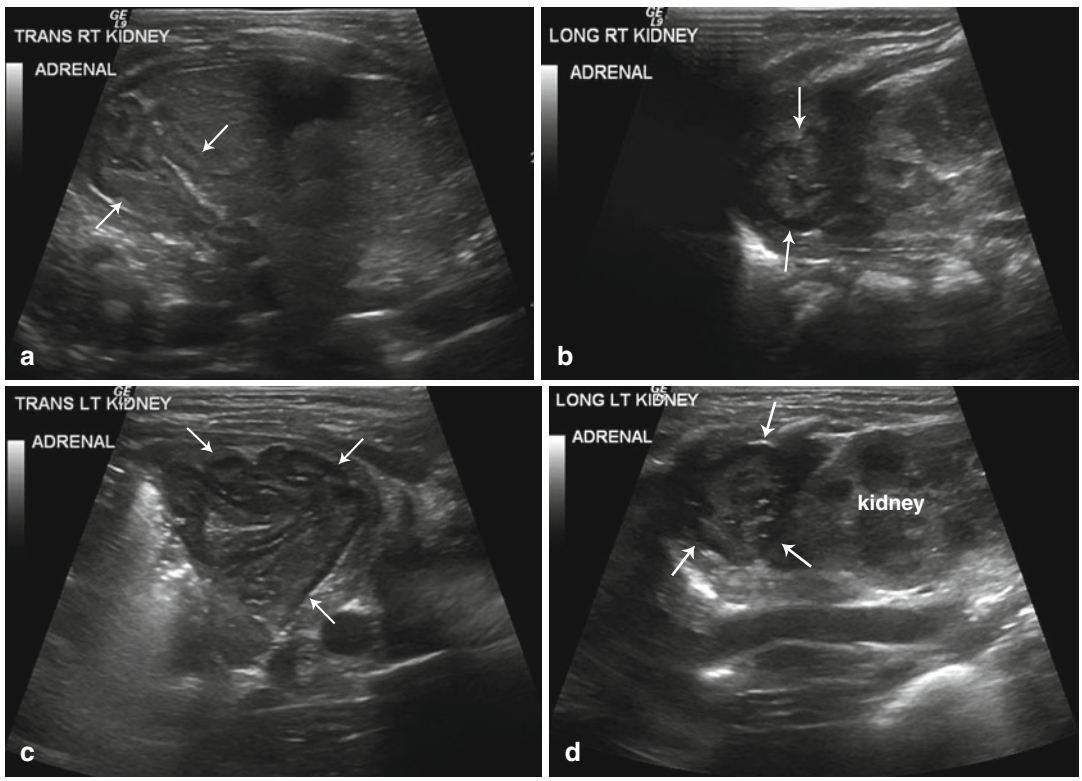

Fig. 16.5 Congenital adrenal hyperplasia. Retroperitoneal ultrasound images from both flanks (**a**–**d**) performed on a newborn girl with ambiguous genitalia due to congenital adrenal hyperplasia reveal enlarged adrenal glands with a cerebriform contour (*arrows*)

Case reports suggest that CAH due to deficiencies in 11β-hydroxylase or 3β-hydroxysteroid dehydrogenase leads to similar changes on adrenal US [20]. Lipoid adrenal hyperplasia is a rare form of CAH due to cholesterol desmolase deficiency, and adrenal glands appear enlarged with echogenicity or attenuation similar to fat due to accumulation of cholesterol and its esters [21].

Adrenal Hyperplasia

When adrenocortical hyperplasia presents in older children, it is classified as primary or secondary [1]. Primary adrenocortical hyperplasia results in either Cushing syndrome or, less commonly, primary hyperaldosteronism (Conn syndrome) [1]. Secondary adrenocortical hyperplasia is due to excess ACTH: either endogenous in those with Cushing disease or ectopic ACTH production or exogenous in those receiving ACTH administration (e.g., for infantile spasms) [1]. Clinical features of Cushing syndrome include central obesity, moon facies, buffalo hump, proximal muscle weakness, easy bruisability, abdominal striae, hypertension, dyslipidemia, insulin resistance, and elevated 24-h urinary cortisol and 17-hydroxycorticoids [22]. Clinical manifestations of Conn syndrome include muscle weakness, hypokalemia, and hypertension [23].

Adrenal glands are not normally visible by US in older children; therefore, if they are visible, the diagnosis of adrenal hyperplasia should be entertained [1]. CT and MR may be used to visualize the adrenals in older children with adrenal hyperplasia. Hyperplastic adrenal glands in these cases will be bilaterally, symmetrically, and evenly enlarged with increased relative enhancement [1]. Alternatively, in some cases of adrenal hyperplasia, adrenal glands may be normal in size, demonstrate uneven enlargement, or contain small nodular areas (Fig. 16.6) [1].

Cushing syndrome and Conn syndrome can also be associated with adrenal adenomas. Benign adrenal adenomas cannot be reliably distinguished from adrenal carcinomas based on histopathology, clinical features, or imaging [24]. However, in general, adrenal adenomas are smaller (<6 cm) compared to adrenal carcinoma and have less heterogeneity on US, CT, and MR. Adrenal carcinomas can have a similar appearance to adrenal adenomas, but tend to be larger and more complex [24]. The only definitive signs of malignancy are hematogenous metastases or venous spread [24].

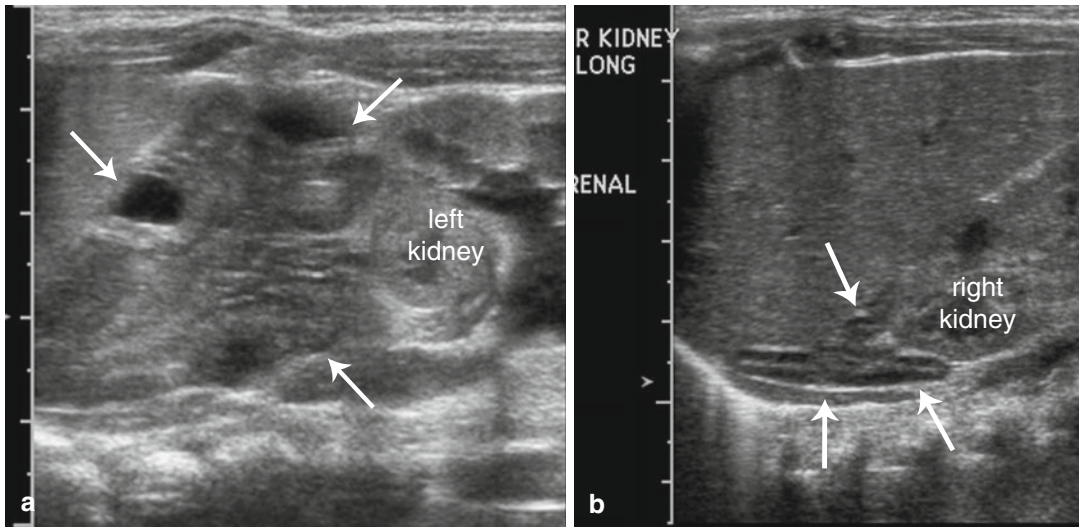

Fig. 16.6 Atypical congenital hyperplasia. US images from the left flank (**a**) reveal an enlarged adrenal gland with a cerebriform contour (*arrows*) and an anatomically normal-appearing adrenal gland from the right flank (**b**)

Primary pigmented nodular adrenocortical disease is a rare form of Cushing syndrome and is associated with Carney complex (Sertoli cell tumors of the testis, cardiac myxomas, soft tissue myxomas, and skin pigmentation) [25]. On imaging, the adrenal gland has multiple, <2 mm cortical-secreting adenomas with atrophic cortex between the nodules [25].

Wolman Disease

Wolman disease, a rare disorder, is an inherited deficiency of lysosomal acid lipase leading to the accumulation of cholesterol esters and triglycerides in many organs, especially in the adrenals [3]. Wolman disease presents in the first few weeks of life with hepatosplenomegaly with abdominal distension, jaundice, vomiting, diarrhea, steatorrhea, anemia, and growth failure and is rapidly progressive leading to death in the first year [3, 5]. On US, the adrenals appear markedly enlarged with calcifications appearing as a long, linear echogenic band with posterior acoustic shadowing [5]. On CT, the adrenals also appear enlarged with a cortical distribution of calcification [5]. Plain film will also demonstrate the densely calcified adrenal gland (Fig. 16.7) [5]. Imaging of adrenals in Wolman disease can look similar to resolving adrenal hemorrhage; however, in adrenal hemorrhage the adrenals are smaller and have globular calcifications [5, 26, 27].

Adrenal Masses

Adrenal masses in children and neonates may be attributable to hemorrhage, neoplasms, cysts, or abscesses [5]. The age and clinical presentation of the child, in conjunction with the imaging features of the mass, will allow one to develop an appropriate list of diagnostic considerations.

In the neonate with an adrenal mass lesion, the most likely entities include adrenal hemorrhage, neuroblastoma, and rarely extralobar pulmonary sequestration. In children less than 5 years of age, neural crest tumors including neuroblastoma and ganglioneuroblastoma are more likely than adrenal hemorrhage and adrenocortical neoplasms except when the child is exhibiting signs and symptoms of a hormonally active tumor. In older children and adolescents, adrenal masses may be related to neural crest tumors (more frequently the mature ganglioneuromas as opposed to neuroblastoma or ganglioneuroblastoma), as well as other tumors including pheochromocytomas and adrenocortical neoplasms. Other rarely seen adrenal masses in children include rhabdoid tumors, myelolipomas, and smooth muscle adrenal tumors [28].

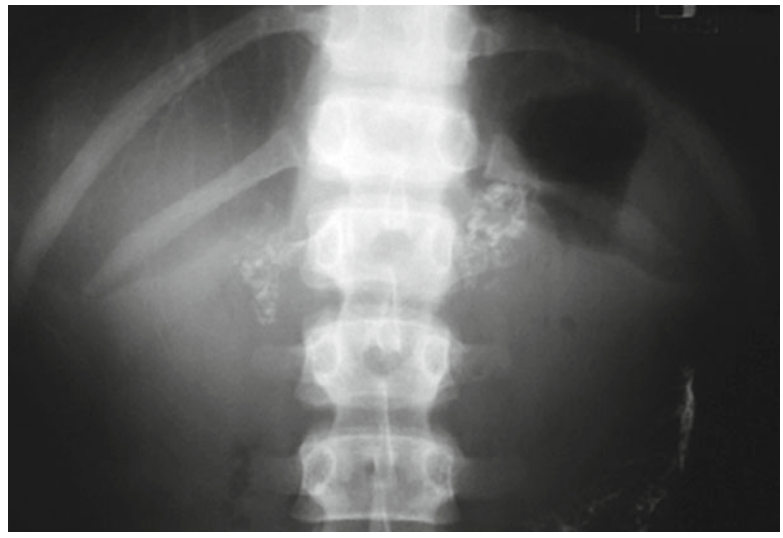

Fig. 16.7 Wolman disease. Abdominal radiograph in a 6-month-old boy reveals calcifications outlining the enlarged adrenal glands, findings typical of Wolman disease

Adrenal Hemorrhage

Adrenal hemorrhage in the perinatal period can occur in response to perinatal stress (such as difficult or traumatic delivery, hypoxia, or sepsis) or bleeding disorders [29]. Large babies such as those of diabetic mothers or with Beckwith-Wiedemann syndrome have a higher predisposition [30]. Associated clinical signs may include palpable flank mass, anemia, jaundice, or rarely hypovolemic shock. However, there is normally no associated adrenal insufficiency in the immediate phase or long-term as the major insult is to the regressing fetal cortex [5]. Beyond the neonatal period, adrenal hemorrhage is frequently seen in the setting of trauma but has also been documented to occur in older children with overwhelming sepsis (specifically *Neisseria meningitidis*), steroid therapy, anticoagulation therapy, and after liver transplantation [5, 11].

Adrenal hemorrhage more often occurs on the right (70 %), and in only 10 % of cases does it occur bilaterally [5]. Hemorrhage size can vary from as small as a few centimeters and up to several centimeters [5]. With conservative management, the natural course of adrenal hemorrhage is central liquefaction with resorption of blood leading to eventual decrease in size to the normal shape and a residual focus of calcification [5].

US is the modality of choice for initial imaging of adrenal masses in neonates as well as for follow-up assessment [31, 32]. On initial US, adrenal hemorrhages have a varied appearance depending on the duration of the hemorrhage. They usually have complex echogenicity with echogenic and echo-free areas but can also appear evenly echogenic, hypoechoic, or anechoic [5]. Smaller hemorrhages may be focal or retain the shape of the adrenal (triangular or crescent-shaped), and adjacent normal adrenal tissue can be identified. Larger adrenal hemorrhages are usually round in shape, and normal unaffected adrenal tissue can be hard to identify (Figs. 16.8a, b) [5]. Large hemorrhages may encompass the upper pole of the kidney (with the appearance of a perinephric hemorrhage) and may track down the retroperitoneum. Clinically, this can lead to scrotal swelling and hematoma, which may mimic testicular torsion [5, 33]. Occasionally, there may be associated ipsilateral renal vein thrombosis, especially on the left since the adrenal vein drains into the left renal vein [5]. To help differentiate adrenal hemorrhage (which is avascular) from neuroblastoma or other adrenal neoplasms, evaluation with color and spectral Doppler assessment should be performed (Fig. 16.8c). Additionally, ultrasound examination should include evaluation of the liver to assess for the presence of hepatic metastases and evaluation of the remainder of the abdomen and pelvis to look for metastatic lymphadenopathy, which can be seen in association with adrenal tumors.

Because of the varied imaging characteristics of adrenal hemorrhage in the acute phase, it may be difficult initially to distinguish from neuroblastoma [34, 35]. Thus, follow-up US imaging is of utmost importance in differentiating a resolving adrenal hemorrhage from a neuroblastoma. Masses due to adrenal hemorrhage decrease in size over several weeks as the hemorrhage liquefies and resorbs and become more hypoechoic or anechoic (Fig. 16.9) [36], whereas in contrast, the size of a neuroblastoma is unlikely to decrease. In cases where the diagnosis is uncertain, a short delay with serial US imaging is not harmful as neonatal neuroblastoma has a relatively good prognosis [11].

In some instances adrenal calcification may be incidentally seen on imaging (plain film, CT, MR) on older children. If the calcification is confined to adrenals of normal size and without evidence for a soft tissue mass, it is assumed to have resulted from previous adrenal hemorrhage in the neonatal period and is of no clinical significance (Fig. 16.10) [5].

In neonates with a suprarenal retroperitoneal mass, the possibility of an intra-abdominal extralobar pulmonary sequestration must also be considered in addition to adrenal hemorrhage and neuroblastoma [3]. Intra-abdominal extralobar pulmonary sequestrations occur more commonly on the left than the right, are usually hyperechoic, and can contain cysts related to coexistent congenital pulmonary airway malformation (Fig. 16.11) [28, 37]. As imaging with US, CT, and MR is rarely diagnostic, surgical diagnosis and treatment is often necessary [38].

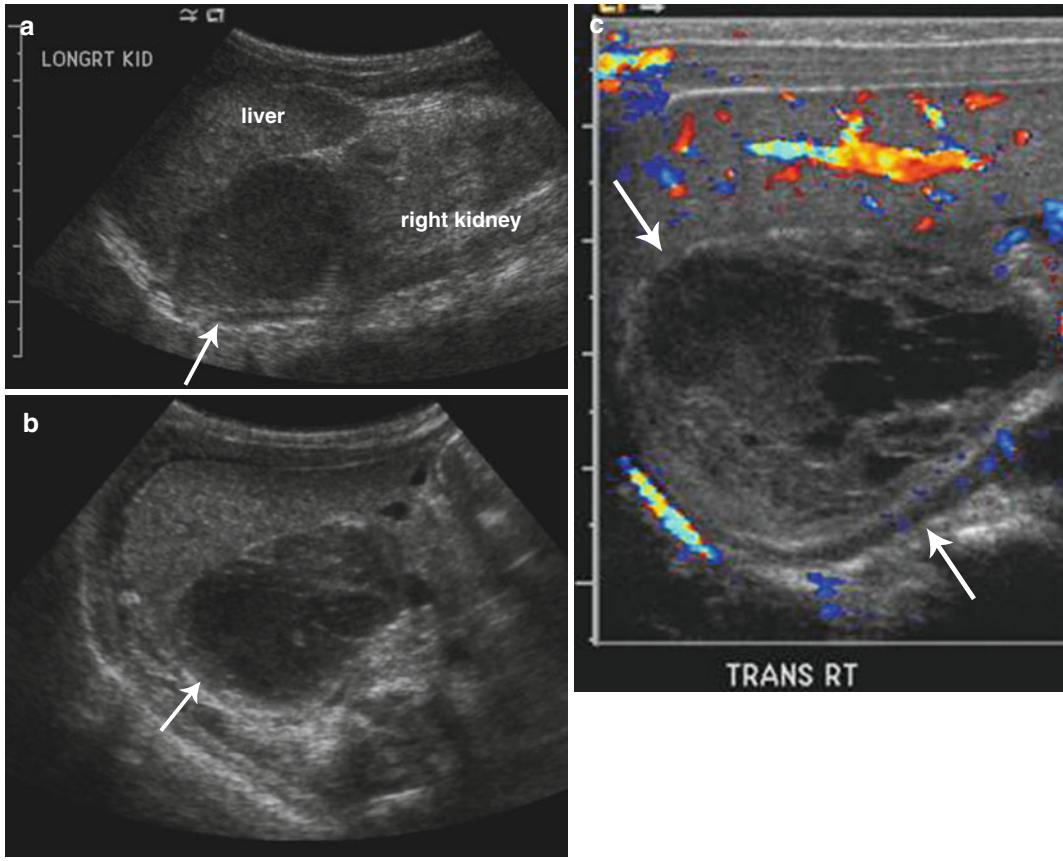

Fig. 16.8 Adrenal hemorrhage. Longitudinal (**a**) and transverse (**b**) ultrasound images in a 2-week-old boy with right adrenal hemorrhage reveal a rounded heterogeneously hypoechoic right adrenal mass (*arrow*). Color Doppler ultrasound image (**c**) shows that the right adrenal mass is avascular (*arrows*) and suggestive of an adrenal hemorrhage

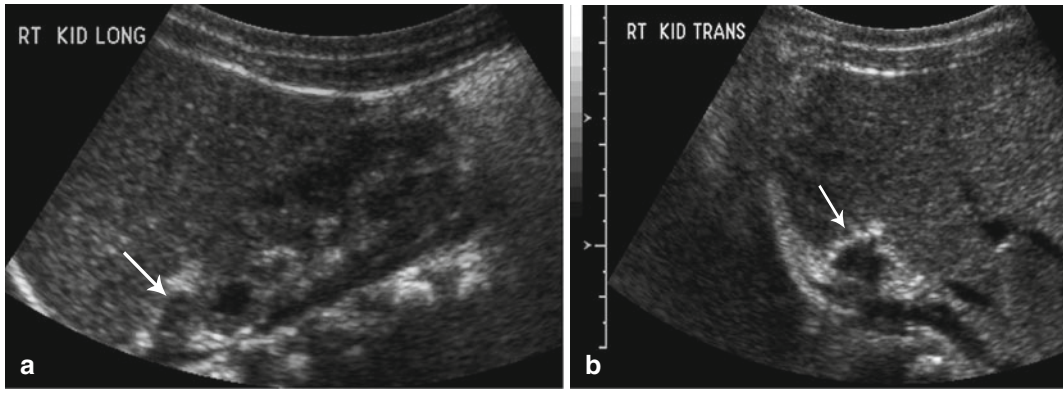

Fig. 16.9 Resolving adrenal hemorrhage. Follow-up longitudinal (**a**) and transverse (**b**) ultrasound images (obtained 2 weeks after the images shown in Fig. 16.8) reveal diminution in the size of the right adrenal gland (*arrows*) and increased peripheral echogenicity (likely early calcification) consistent with a resolving adrenal hemorrhage

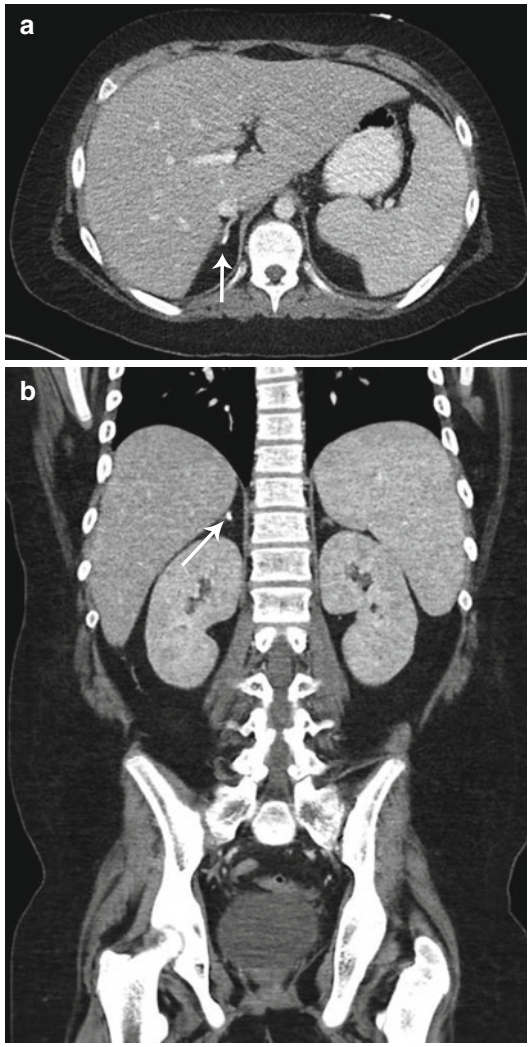

Fig. 16.10 Old adrenal hemorrhage. Axial (**a**) and coronal (**b**) contrast-enhanced CT images of the abdomen in a 10-year-old boy reveal a small focus of calcification in the right adrenal gland (*arrows*) with no associated soft tissue mass, presumed the sequela of prior adrenal hemorrhage

Medullary Neoplasms

Medullary adrenal neoplasms include the neuroblastoma, ganglioneuroblastoma, ganglioneuroma, and pheochromocytoma. These can occur within the medulla of the adrenal gland but also along the sympathetic nervous chain [1].

Neuroblastoma

Neuroblastoma, ganglioneuroblastoma, and ganglioneuroma are tumors which arise from the neural crest cells of the sympathetic nervous system [39]. Neuroblastomas are malignant tumors composed of immature neuroblasts. Ganglioneuroblastomas are composed of both immature and mature cells and have malignant potential. Ganglioneuromas composed entirely of mature gangliocytes and mature stroma are benign [39].

Neuroblastoma represents 8–10 % of all childhood cancers making it the most common extracranial solid tumor of childhood [39–41]. The median age of neuroblastoma diagnosis is 19 months, most present between 1 and 5 years of age [3]. Most primary tumors are in the abdomen (65 %), although children have a higher frequency of adrenal tumors than infants (40 % vs. 25 %). The remaining abdominal and pelvic tumors mostly originate in the paravertebral sympathetic ganglia or in the presacral area from the organ of Zuckerkandl [3].

Most children present with abdominal pain or a palpable mass, but others are identified by manifestations of their metastatic disease, as up to 70 % of patients have metastases at presentation [3]. Patterns of metastases vary with age at presentation, and locations can include lymph nodes, liver, skeleton, bone marrow, and skin [3]. Neonates and younger infants more commonly have cutaneous lesions (blueberry muffin syndrome) and extensive hepatic involvement (however, hepatic metastases can occur at any age), whereas older infants and children more commonly have skeletal metastases [3]. Additionally, patients may present with paraneoplastic syndromes. Serum or urinary levels of catecholamines or their metabolites (vanillylmandelic acid (VMA), homovanillic acid (HVA)) are increased in 90 % of children with neuroblastoma [42]; however, secretion of catecholamines rarely leads to symptoms such as those seen in pheochromocytoma: paroxysmal hypertension, palpitations, flushing, and headaches. Secretion of catecholamines or vasoactive intestinal peptide (VIP) may lead to severe watery diarrhea, hypokalemia, and acidosis [43]. Additionally, one can present with acute myoclonic encephalopathy comprised of myoclonus, opsoclonus (rapid multidirectional eye movements), and cerebellar ataxia; this is thought to be due to an immune response to the primary tumor leading to production of anti-neural antibodies that cross-react with cerebellar tissue [44].

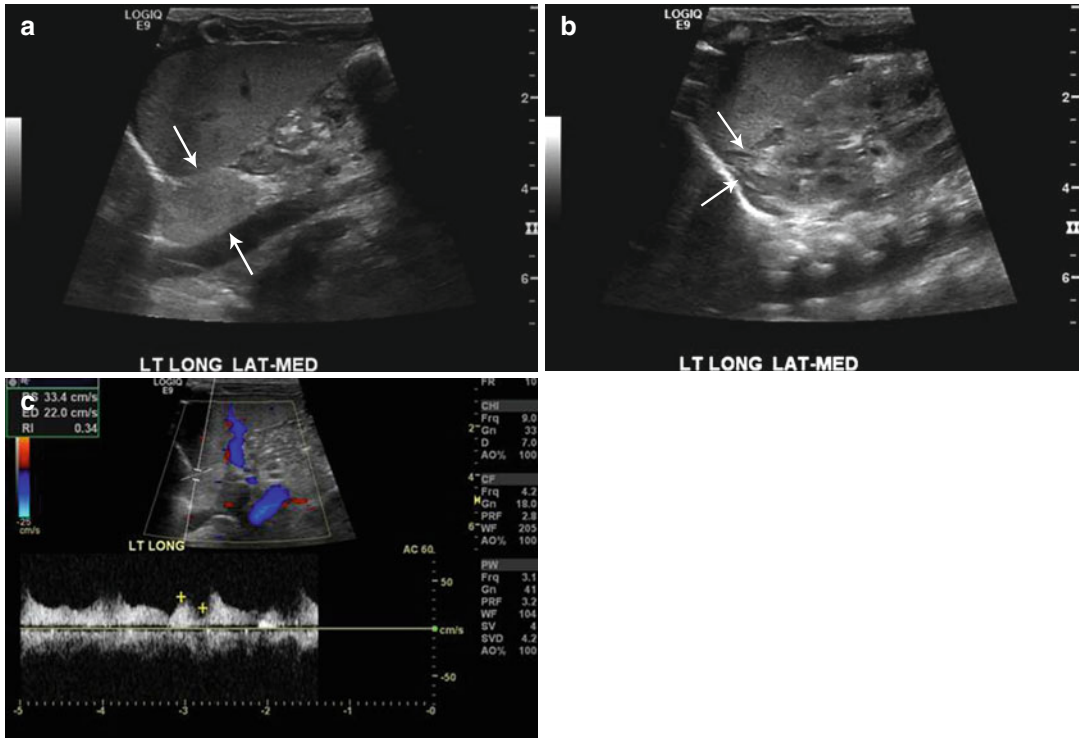

Fig. 16.11 Retroperitoneal extralobar pulmonary sequestration. Longitudinal ultrasound images of the left upper abdomen (**a**) in an 11-day-old boy with prenatally diagnosed mass reveal an echogenic mass medially (*arrows*) and a normal-appearing adrenal gland laterally (**b**). Doppler assessment confirmed internal blood flow (**c**) with large systemic artery typical for an extralobar pulmonary sequestration

Table 16.1 International neuroblastoma staging system

Stage	Description
1	Localized tumor with complete gross excision, with or without microscopic residual disease; representative ipsilateral lymph nodes negative for tumor microscopically
2A	Localized tumor with incomplete gross excision; representative ipsilateral nonadherent lymph nodes negative for tumor microscopically
2B	Localized tumor with or without complete gross excision, with ipsilateral nonadherent lymph nodes positive for tumor. Enlarged contralateral lymph nodes must be negative microscopically
3	Unresectable unilateral tumor infiltrating across the midline, with or without regional lymph node involvement; localized unilateral tumor with contralateral regional lymph node involvement; or midline tumor with bilateral extension by infiltration (unresectable) or by lymph node involvement. The midline is defined as the vertebral column. Tumors originating on one side and crossing the midline must infiltrate to or beyond the opposite side of the vertebral column
4	Any primary tumor with dissemination to distant lymph nodes, bone, bone marrow, liver, skin, and/or other organs, except as defined for stage 4S
4S	Localized primary tumor, as defined for stage 1, 2A, or 2B, with dissemination limited to skin, liver, and/or bone marrow (limited to infants younger than 1 year). Marrow involvement should be minimal (i.e., <10 % of total nucleated cells identified as malignant by bone biopsy or by bone marrow aspirate). More extensive bone marrow involvement would be considered stage 4 disease. The results of the metaiodobenzylguanidine (MIBG) scan, if performed, should be negative for disease in the bone marrow

Adapted from Brodeur et al. [45]

The prognosis of neuroblastoma is related to age, stage at presentation (see Table 16.1), and tumor site [1]. According to the International Neuroblastoma Staging System (INSS), the distribution at presentation is as follows: stage 1, 17 %; stage 2A/2B, 16 %; stage 3, 16 %; stage 4,

44 %; and stage 4S, 7 % [41]. However, newer staging systems based on imaging, instead of surgical, findings are in development [46]. Favorable prognosis occurs in patients <1 year of age, low-stage disease at presentation, and tumors arising from extra-abdominal sites. For example, 2-year survival is 80 % in patients with localized disease, whereas it is less than 5 % for patients with skeletal metastases [11]. Additionally, poor prognostic signs are N-myc amplification (>10 copies), allelic loss of chromosome 1p, and diploid karyotype, whereas favorable prognostic factors are unamplified N-myc oncogene, absence of abnormalities on chromosome 1p, triploid karyotype, and well-differentiated stroma on histology [39].

Treatment consists of a combination of surgery, chemotherapy, and radiation depending on the stage at presentation. Primary surgical resection is used for more localized tumors and chemotherapy for unresectable lesions or in a neoadjuvant setting to shrink lesions sufficiently for delayed surgical resection [39].

Neuroblastomas (and ganglioneuroblastoma) have varied appearance by US [3, 39]. They appear either as a suprarenal or paraspinal masses with the retroperitoneal location evident by anterior displacement of the inferior vena cava or aorta or displacement of retroperitoneal organs [3]. On US, neuroblastomas may be homogeneous or heterogeneous in echogenicity with hyperechoic areas of calcification (often without acoustic shadowing) and hypoechoic areas due to a combination of hemorrhage, necrosis, and cystic change (Fig. 16.12) [39]. In newborns, neuroblastomas may instead be hypoechoic or mainly cystic [11]. Doppler US may be used to confirm the presence of blood flow in the mass and to evaluate patency of encased vessels [39, 40].

Cross-sectional imaging for staging of neuroblastoma is needed in order to assess the organ of origin, extent of the tumor, local invasion, vascular encasement or displacement, calcification, lymphadenopathy, and metastases [24, 47]. On CT, neuroblastoma lesions have attenuation similar or less than that of the muscle [1]. Calcification is present in up to 85 % of cases and may be finely stippled, curvilinear, coarse, or globular [1]. With intravenous contrast, neuroblastoma lesions enhance heterogeneously demonstrating

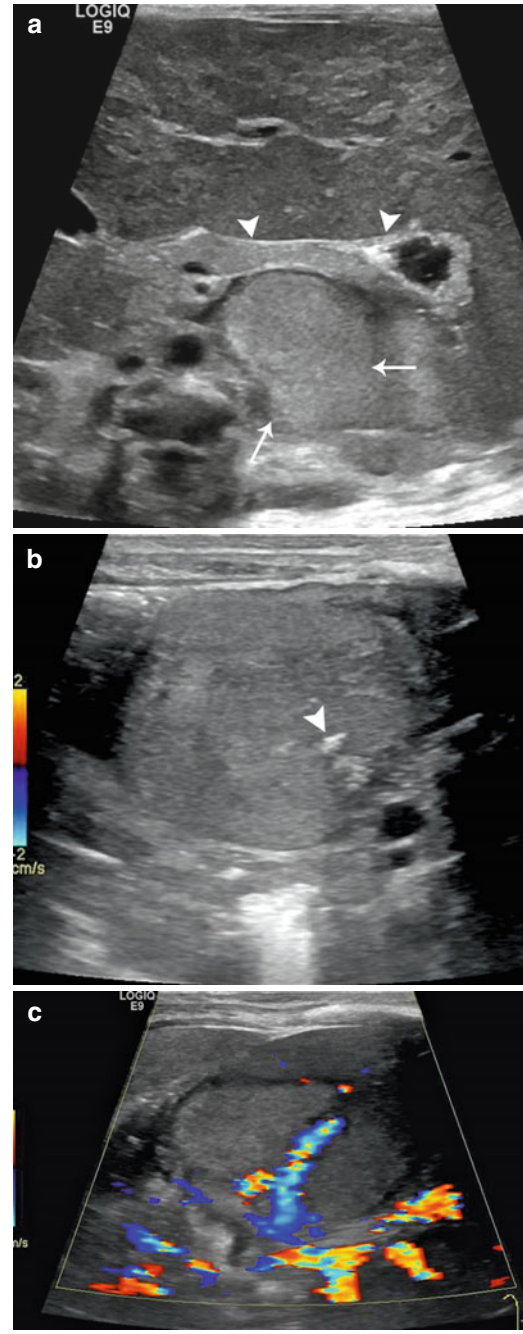

Fig. 16.12 Neuroblastoma – *US.* Transverse ultrasound image of the upper abdomen (**a**) in this neonate reveals a solid-appearing mass arising from the left adrenal gland (*arrows*) which displaces the pancreas (*arrowhead*) anteriorly. On focused ultrasound image (**b**) the left adrenal mass contains echogenic foci (*arrowheads*) due to calcifications. Color Doppler image of the left adrenal mass (**c**) demonstrates internal vascularity (*arrow*) unlike the appearance of an adrenal hemorrhage (See Fig. 16.8)

areas of vascularity and low attenuation regions up to 4 cm in diameter representing necrosis or hemorrhage (Fig. 16.13) [1]. On MR, neuroblastomas are often heterogeneous with variable enhancement. On T1-weighted images, lesions have low to intermediate signal intensity and high signal intensity on T2-weighted and fat-suppressed images [1]. Cysts and areas of necrosis are hypointense on T1-weighted images and hyperintense on T2-weighted images; these areas do not demonstrate enhancement with gadolinium. Areas of calcification demonstrate hypointensity on all MR sequences (Fig. 16.14) [11].

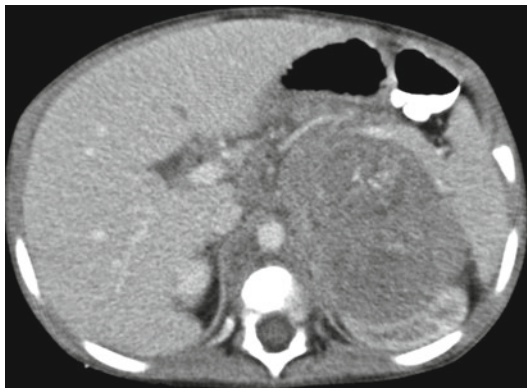

Fig. 16.13 Neuroblastoma – *CT.* Contrast-enhanced axial CT images in an 18-month-old boy with an adrenal gland origin neuroblastoma compressing and displacing the adjacent kidney

CT or MR should also be used to determine the full extent of the tumor within the abdomen. Vascular encasement and compression can be seen of the inferior vena cava, aorta, celiac artery, superior mesenteric artery, renal vessels, and splenic vein; hypertension may result from renal vascular compression (Fig. 16.13) [39]. Renal hilar, porta hepatis, and retroperitoneal lymphadenopathy may be demonstrated [39].

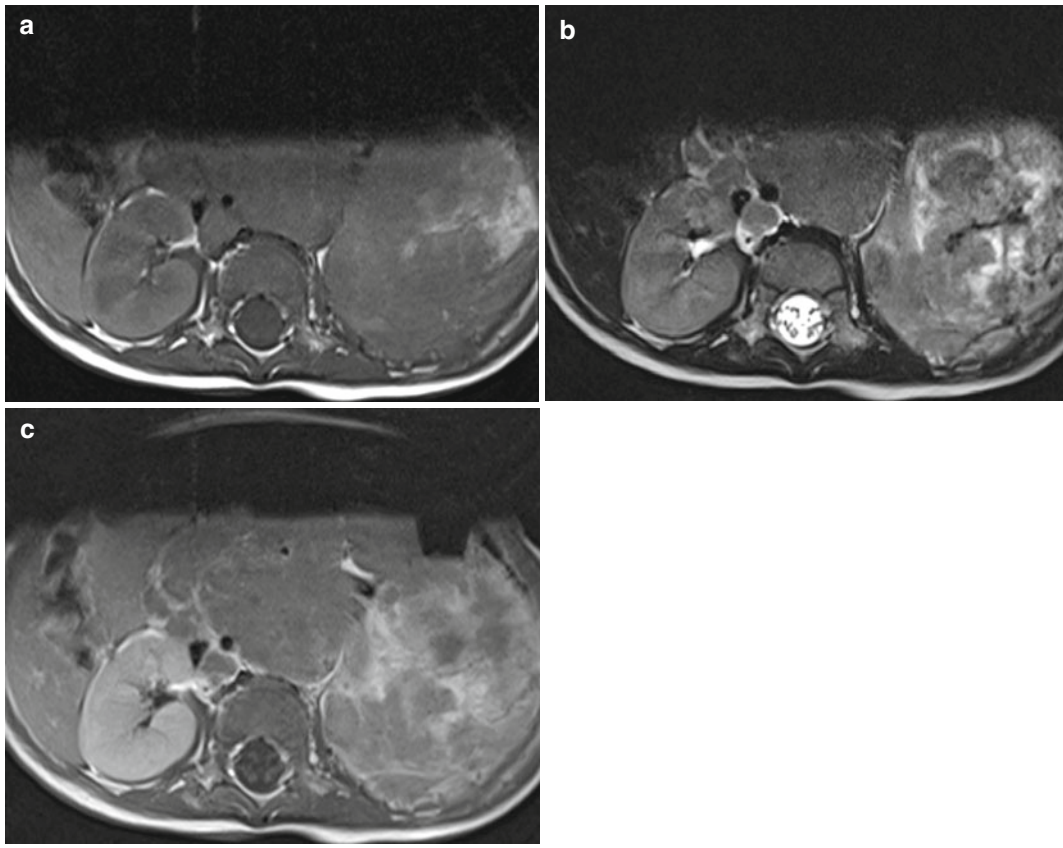

Fig. 16.14 Neuroblastoma – *MR.* MR images in a 5-year-old boy with a left adrenal neuroblastoma reveal heterogenous intermediate T1 signal (**a**) and mixed intermediate and increased T2 intensity (**b**) and patchy enhancement following contrast enhancement with gadolinium (**c**)

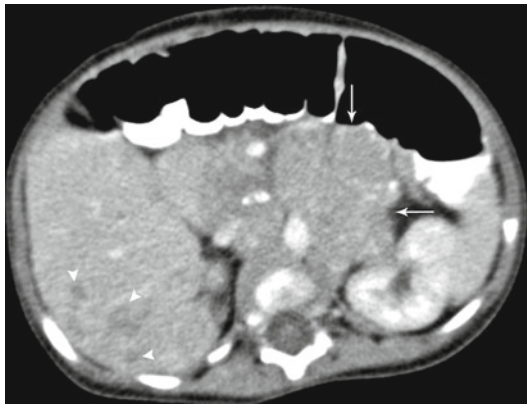

Fig. 16.15 Neuroblastoma. Contrast-enhanced axial CT images in a 5-month-old girl with stage 4S Neuroblastoma (*arrows*). CT image reveals a heterogeneously enhancing left adrenal mass (*arrows*) and multiple low attenuation liver metastases (*arrowheads*)

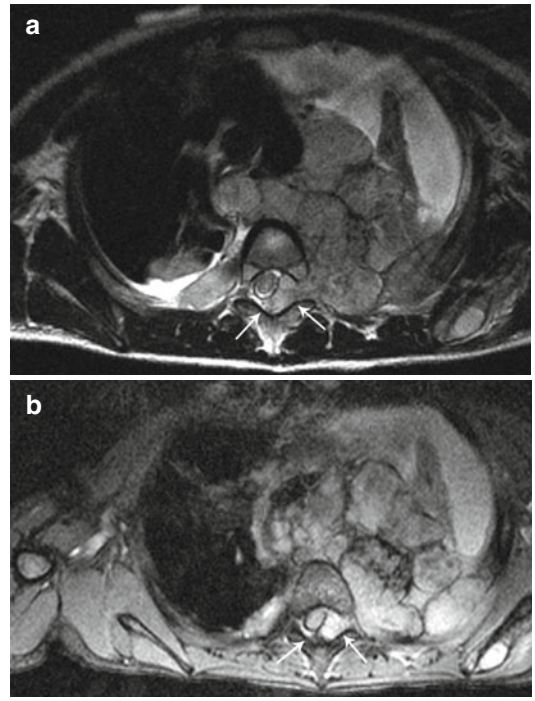

Fig. 16.16 Neuroblastoma. Axial MR images (**a**, **b**) in a 5-year-old boy with a large posterior mediastinal neuroblastoma demonstrates evidence of tumor extension into the spinal canal (*arrows*) with associated displacement and compression of the spinal cord

Metastases into the liver, lung, lymph nodes, and brain can be demonstrated by both CT and MR (Fig. 16.15) [39]. Imaging should be assessed for direct invasion into the kidneys, liver, psoas, paraspinal muscles, and epidural space; MR may more easily demonstrate locoregional invasion (Fig. 16.16) [39]. MR is superior to CT for visualization of the intraspinal tumor extension and bone marrow infiltration (Fig. 16.16) [39, 48].

In addition to cross-sectional imaging, patients with neuroblastomas and ganglioneuroblastomas routinely undergo metaiodobenzylguanidine (MIBG) scans to evaluate for sites of metastatic disease. MIBG is taken up by catecholamine-producing tumors including neuroblastomas, ganglioneuroblastomas, and ganglioneuromas [39]. Greater than 90 % of neuroblastomas are MIBG avid [49]. Other tumors which are typically MIBG avid include pheochromocytomas, carcinoid tumors, and medullary thyroid carcinomas [39]. MIBG scintigraphy is highly sensitive for the detection of metastatic bone disease, allowing visualization of both cortical and bone marrow metastatic disease [39]. Alternatively, Tc-99m methylene diphosphonate (MDP) bone scans can be used to detect bone metastases (Fig. 16.17).

Positron emission tomography (PET) with the glucose analogue ^{18}F fluorodeoxyglucose (FDG) currently has a limited role in the evaluation of neuroblastoma because MIBG is more sensitive for the detection of neuroblastoma [49]. ^{18}F-FDG PET scans may be helpful for the evaluation of MIBG-negative neuroblastomas as well as stage 1 and 2 neuroblastomas (Fig. 16.18) [50]. Additionally, ^{18}F-FDG PET scans are recommended when cross-sectional (CT and MR) imaging studies suggest greater extent of disease than seen on MIBG imaging. Another positron emitting imaging agent, ^{18}F dihydroxyphenylalanine (DOPA) which is not yet widely available, has shown promise in initial studies of patients with stage 3 and 4 neuroblastoma when compared to ^{123}I-MIBG [51].

Ganglioneuroma

In comparison to neuroblastomas, ganglioneuromas are benign completely differentiated tumors of mature ganglion cells [11]. Ganglioneuromas may arise de novo, develop from maturing neuroblastoma or ganglioneuroblastoma, or arise from treated neuroblastoma or ganglioneuroblastoma [1]. In contrast to neuroblastoma, ganglioneuromas are more often found in asymptomatic older

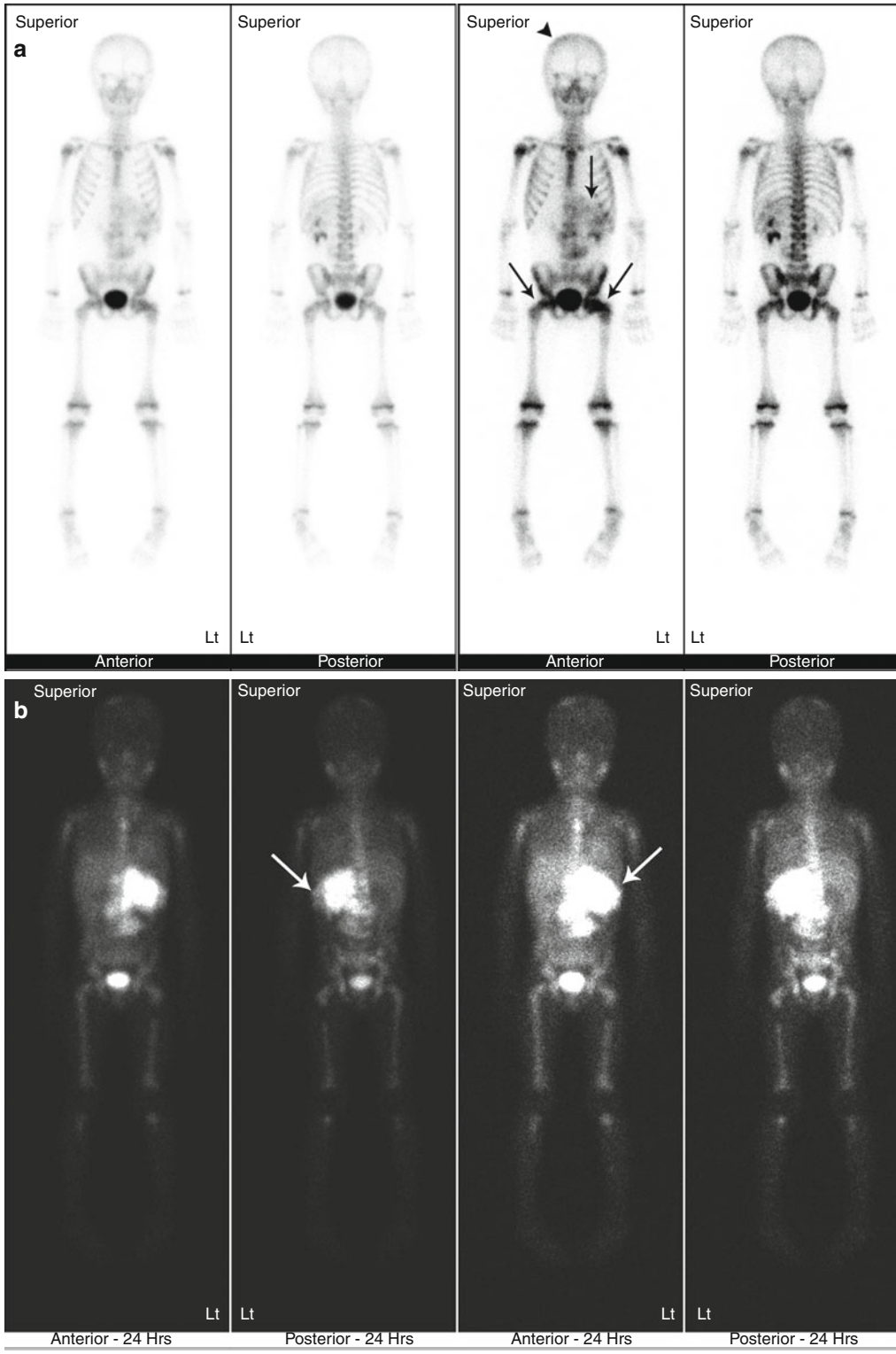

Fig. 16.17 Neuroblastoma. Bone scan (**a**) and MIBG scan (**b**) were performed in a 3-year-old boy with stage 4 neuroblastoma. Abnormally increased radiotracer localization on the bone scan (**a**) is seen in the skull (*arrowhead*), primary left retroperitoneal mass (*arrows*), and proximal femurs bilaterally (*arrows*). MIBG scan (**b**) shows evidence of extensive metastatic disease in the bone and bone marrow and in the primary left retroperitoneal tumor (*arrow*). All of the visualized skeletal activity on the MIBG scan represents sites of metastatic bone and/or bone marrow disease

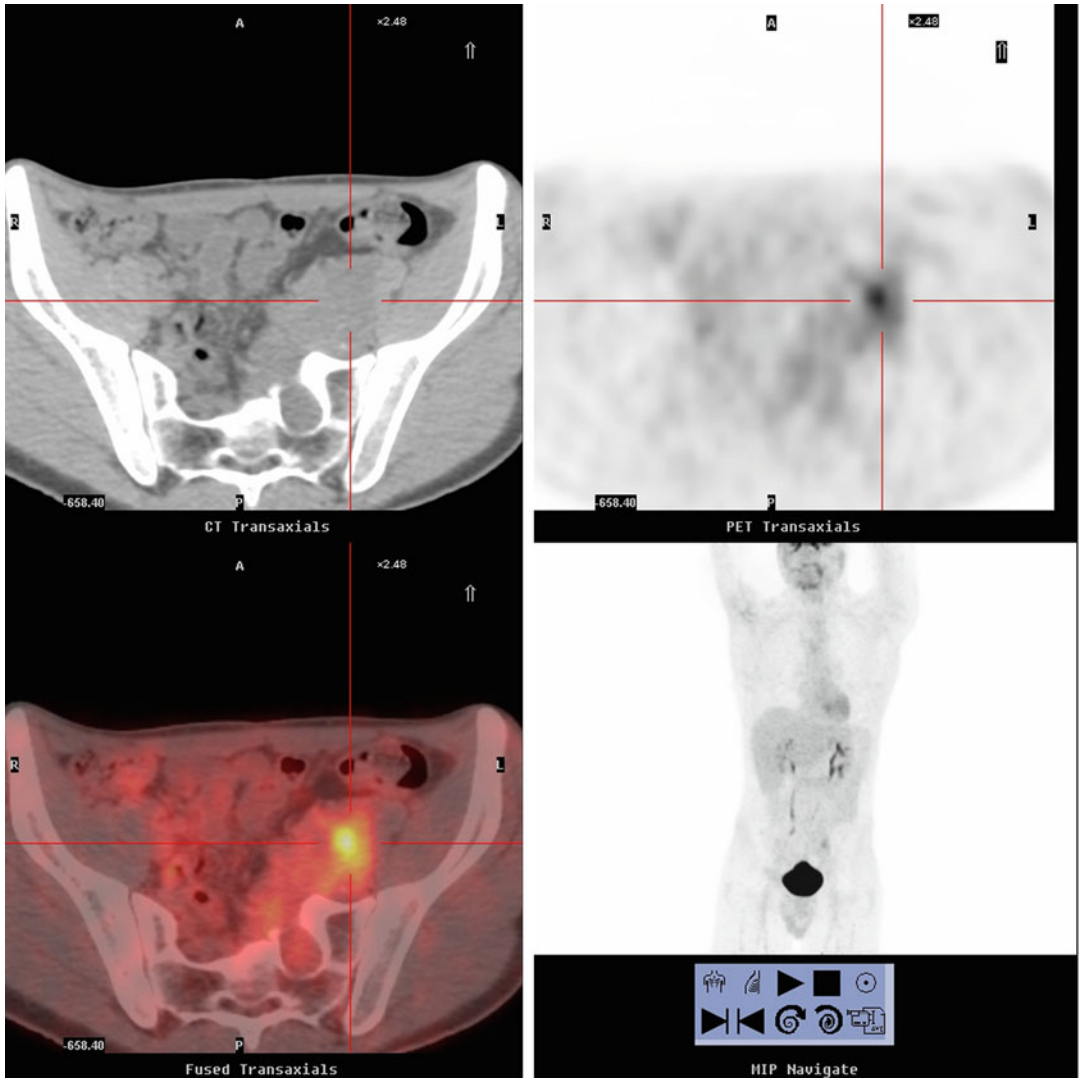

Fig. 16.18 Neuroblastoma. PET/CT scan in a 17-year-old boy with a left presacral neuroblastoma (centered in the crosshairs) on localizing noncontrast CT (labeled CT transaxials) with increased metabolic activity on the PET (labeled PET transaxials) and fused PET/CT (labeled fused transaxials) images

children (median age of 7) as an incidental finding on imaging performed for other reasons [1]. Most ganglioneuromas arise in the posterior mediastinum, and only one-third arise in the abdomen (mostly paravertebral, less frequently suprarenal) (Fig. 16.19) [1]. As ganglioneuroma appearance on imaging is similar to that of neuroblastoma, diagnosis is made by histologic examination of tumor tissue [1]. A needle biopsy is not sufficient due to sampling error and cannot reliably confirm benign histology throughout the entire lesion. Treatment consists of complete surgical resection when possible with subsequent periodic radiologic surveillance; if surgical removal is not possible (large tumors, involvement of vessels or other vital structures, or extension into the intervertebral foramina), patients should be followed for life to monitor for development of malignant peripheral nerve sheath tumors [1].

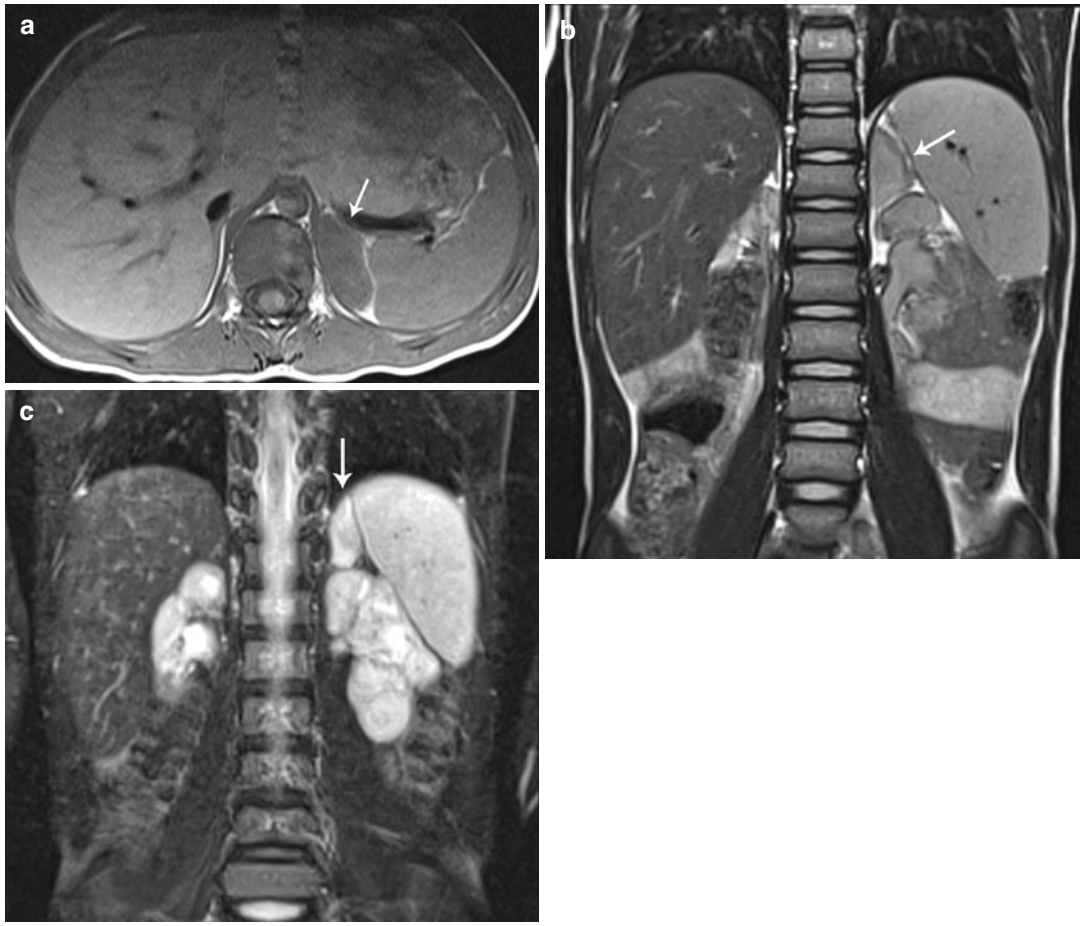

Fig. 16.19 Ganglioneuroma. MR scans ((**a**) axial T1, (**b**) coronal T1, (**c**) coronal T2) in a 5-year-old boy with history of neurogenic bladder and bilateral ureteral reflux revealed an adrenal mass (*arrows*). This proved to be a benign left adrenal ganglioneuroma

Pheochromocytoma

Pheochromocytoma is a functionally active catecholamine-secreting tumor involving chromaffin cells of the sympathetic nervous system. Most originate in the adrenal medulla; however, up to 30 % are extra-adrenal (termed paragangliomas) in locations such as the paravertebral sympathetic chain, para-aortic bodies, bladder wall, spermatic cord, or vagina [1, 3]. Pheochromocytoma is an uncommon neoplasm in children as only 5 % of all pheochromocytomas occur in children and they represent under 1 % of childhood neoplasms [1]. In children, 70 % of pheochromocytomas arise in the adrenal gland and 24 % are bilateral [1]. There is a higher incidence of pheochromocytoma (in addition to multiple and/or bilateral tumors) in patients with multiple endocrine neoplasia (MEN) type 2 (with medullary thyroid carcinoma and parathyroid hyperplasia), tuberous sclerosis, neurofibromatosis, hemihypertrophy, Sturge-Weber syndrome, and von Hippel-Lindau disease [3]. Clinical manifestations of pheochromocytomas are due to epinephrine and norepinephrine release, and include paroxysmal hypertension, tachycardia, sweating, flushing, headaches, blurred vision, papilledema, hypertensive encephalopathy, diarrhea, weight loss, and micturition syncope (in the case of bladder wall paragangliomas) [1]. Diagnosis is made with elevated levels of plasma or urinary levels of

catecholamines or their metabolites (vanillylmandelic acid [VMA], homovanillic acid [HVA]) [3].

Imaging is necessary to localize the primary lesion(s) and any sites of metastatic spread to allow for treatment via surgical removal [3, 40]. Pheochromocytomas can range in size from 1 to 10 cm at presentation; however, most are between 2 and 5 cm [1]. On US, pheochromocytoma lesions can be homogeneously or heterogeneously echoic with hypoechoic areas of hemorrhage and necrosis and hyperechoic areas of hemorrhage and calcification. Smaller pheochromocytomas are more likely to be homogeneous and larger lesions heterogeneous [1, 3]. On CT, pheochromocytomas have soft tissue attenuation, and enhancement may be diffuse, heterogeneous, or rim-enhancing (Figs. 16.20a, b) [1]. On MR T1-weighted images, pheochromocytomas are

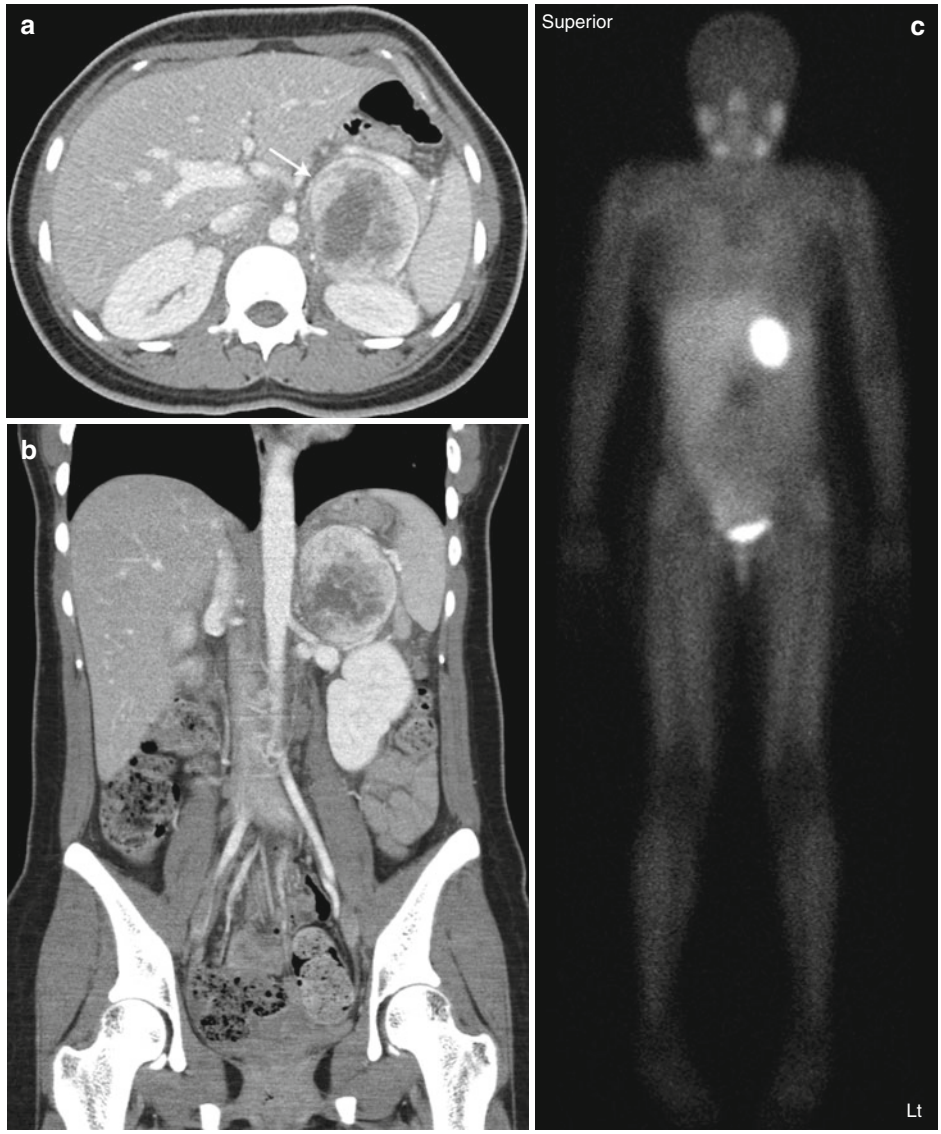

Fig. 16.20 Pheochromocytoma. Axial (**a**) and coronal (**b**) contrast-enhanced CT images and MIBG scan (**c**) performed in a teenage girl with history of tachycardia and hypertension reveal a heterogeneously enhancing left adrenal mass (*arrows*) on CT which is strongly MIBG avid on MIBG scan (**c**) and was confirmed to be a pheochromocytoma

hypointense to the liver; on T2-weighted and fat-suppressed images, pheochromocytomas are hyperintense to the liver and fat [11]. Of note, they show a higher signal intensity compared to adrenocortical tumors. After gadolinium infusion, these lesions have moderate to marked heterogeneous enhancement with a slow washout period [1, 11]. Whole body MIBG scintigraphy can also be used to localize lesions and metastatic sites (Fig. 16.20c) [1].

Adrenocortical Neoplasms

Adrenocortical tumors are not common in children. The majority of these lesions are hyperfunctioning hormone-producing tumors with the most common abnormality being the overproduction of androgens [24, 52]. Girls present with signs of virilization including facial hair, advanced pubic and axillary hair development, advanced bone age, increased muscle mass, and clitoromegaly [24]. While boys present with signs of isosexual pseudoprecocious puberty including early acne, pubic hair, and penile enlargement [24]. In the rare nonfunctioning lesions, a child may present with an abdominal mass or incidental finding on imaging. Girls are more commonly affected than boys, in a 2–3:1 ratio. Carcinomas are more common than adenomas [1, 24]. Adrenocortical neoplasms are less common than neuroblastoma but more common than pheochromocytoma [28].

Unfortunately, compared to adult tumors, pediatric adrenal adenoma and adrenal carcinoma are difficult to distinguish histopathologically [24]. In adults, adrenal adenomas have a low nuclear-to-cytoplasmic ratio with very little necrosis or hemorrhage and rare mitoses; however, in children, these tumors are more likely to show nuclear atypia, pleomorphism, necrosis, and mitotic activity [24]. In comparison, adrenal carcinomas have a wide range of morphology from normal-appearing adrenal cells to completely undifferentiated cells [24]. Multiple attempts have been made to classify adrenal adenomas vs. adrenal carcinomas based on tumor size, clinical findings, and histopathologic features. However, these two lesions cannot be reliably differentiated based on these systems [24, 52]. Only the detection of metastases can distinguish malignant tumors from benign lesions.

Adrenocortical Carcinoma

Adrenocortical carcinoma is a malignant neoplasm of the adrenal cortex and is quite rare, accounting for <1 % of all pediatric malignancies [24, 52]. Most present at a mean age of 9 years with androgen overproduction (virilization in girls, pseudoprecocious puberty in boys) as seen by elevated urinary 17-ketosteroids and normal to slightly elevated urinary cortisol levels [3]. Unusual presentations include pure Cushing syndrome, hyperaldosteronism leading to hypertension, or estrogen secretion leading to feminization on boys [24]. There is an association between adrenal cancer and hemihypertrophy, Beckwith-Wiedemann syndrome, and Li-Fraumeni syndrome [24]. As stated above, definitive diagnosis of adrenal adenoma vs. carcinoma cannot be made on imaging characteristics, biochemical criteria, or even histopathologically; however, larger or palpable lesions are more likely to be carcinoma [1]. Adrenal carcinoma may locally invade the kidney, renal vein, or inferior vena cava; distant metastases are most common in the lungs, liver, peritoneum, pleura, diaphragm, abdominal lymph nodes, and kidney [24]. Treatment consists of complete resection with adjuvant chemotherapy reserved for metastases, recurrent disease, or persistently elevated hormones after resection [24]. Survival is related to age at presentation: Lack et al. demonstrated a 13 % survival rate for children older than 5 years and 70 % for children 5 years or younger (combined adrenal carcinoma and adenoma cases) [53].

Adrenal carcinomas are normally large at presentation, mostly greater than 5 cm, but can vary in size [24, 52]. On US, larger lesions are usually heterogeneous with necrosis, hemorrhage, and calcification (in up to 40 %) leading to hypoechoic or hyperechoic areas [3]. Smaller lesions may be more homogeneous in nature (Fig. 16.21a) [3]. US Doppler imaging may be used to detect venous tumor thrombus [3]. On CT and MR, larger lesions also appear more heterogeneous

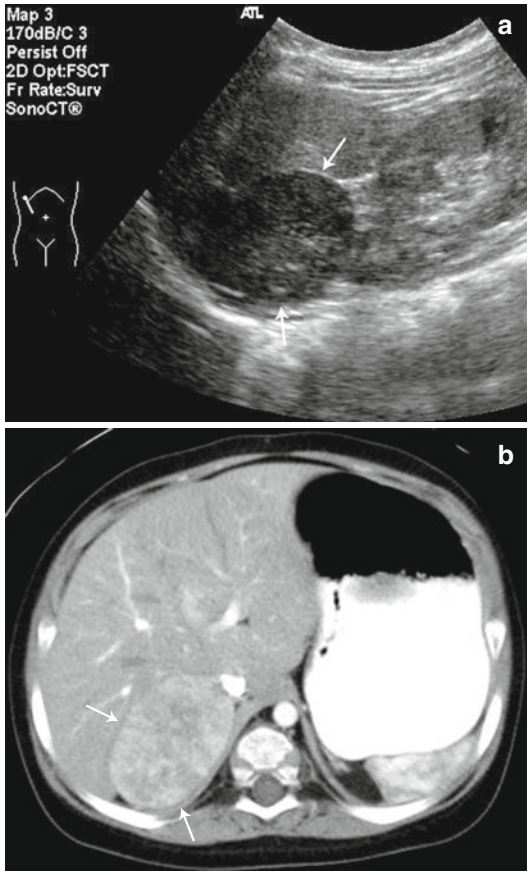

Fig. 16.21 Adrenocortical neoplasm. US (**a**) and CT (**b**) images through the upper abdomen reveal a solid soft tissue mass (*arrows*) found to be an adrenocortical neoplasm

compared to the homogeneous smaller lesions. Larger lesions may have a central scar with radiation linear bands representing areas of calcification and necrosis (Fig. 16.21b) [1]. On MR, adrenal lesions (adenomas and carcinomas) tend to be intermediate signal intensity on T1-weighted images and high signal intensity compared to the liver on T2-weighted images [24]. CT and MR are superior to US in assessing for local invasion and metastatic spread and are of paramount importance when assessing for inferior vena cava tumor thrombus which may involve a thoracoabdominal surgical approach for intrahepatic or right atrial tumor thrombus [24]. ^{18}F-FDG PET scan can be used to locate distant metastases or tumor recurrence not detected on CT or MR. Additionally, Tc-99m MDP bone scans can be used in the initial evaluation to detect bone metastases in those limited cases. As noted, the diagnosis of malignancy is characterized by local spread, invasion, and metastatic disease, not histopathology or primary mass imaging characteristics [24, 52].

Other Adrenal Neoplasms

Leiomyomas

Leiomyomas, smooth muscle tumors, have been described to occur in the adrenal glands, gastrointestinal, tracheobronchopulmonary, and hepatobiliary symptoms in pediatric acquired immunodeficiency syndrome (AIDS) in association with Epstein-Barr virus (EBV) [54]. They are usually unilateral, but can be bilateral and are thought to arise from adrenal vasculature smooth muscle [1]. Most leiomyomas within the adrenal gland are small and benign appearing by imaging (i.e., homogeneous). However, some leiomyomas are larger and more complex on US, CT, and MR, and they have inconsistent ^{18}F-FDG PET avidity; therefore, the recommendation is surgical removal for those >6 cm [55].

Myelolipoma

Myelolipomas are cortical, nonfunctioning, benign tumors that are rare, mostly unilateral, and most often found in the adrenal gland. These lesions are more common in adults (frequently in the fifth–seventh decades), but are rarely seen in children [56]. Tumors are usually small and asymptomatic and found incidentally on imaging. Myelolipomas are composed of fat and bone marrow components, and on US the fat components are highly echogenic and myeloid components are hypoechoic or isoechoic to adrenal parenchyma [3]. On CT, the fat component is easily identified by regions of low Hounsfield unit (HU) attenuation (−30 to −100 HU) [57]. MR can be used to confirm adrenal origin by defining tissue planes, and lipid-containing regions can be identified by high signal intensity on T1-weighted images, intermediate signal intensity on T2-weighed images, and loss of signal intensity on fat suppression scans [57]. Treatment is usually conservative when patients are asymptomatic.

Adrenal Cysts

Cysts in the adrenal gland can form in multiple disease states. Adrenal cysts can form during resolution of neonatal adrenal hemorrhage [5]. Additionally, neuroblastoma can present in a cystic form prenatally or in the neonate [5]. Beckwith-Wiedemann syndrome and hemihypertrophy may be associated with adrenal microcysts located in the capsule or superficial adult cortex [5]. These microcysts can undergo exaggerated development leading to macroscopic adrenal cysts at birth. Macroscopic adrenal cysts associated with Beckwith-Wiedemann syndrome are usually unilateral and large (up to several centimeters), may be multiloculated, and are usually hemorrhagic [5]. Treatment is conservative as they shrink and may disappear with time [58].

On US, adrenal cysts are round anechoic masses with well-circumscribed thin walls and through-sound transmission [3]. However, septations, fluid-fluid levels, wall calcification, and multilocular cystic masses can also occur [3]. Other suprarenal, but extra-adrenal, cysts due to bronchogenic foregut malformations, such as bronchogenic cysts, cystic adenomatoid malformation, intra-abdominal sequestration with cystic elements, and esophageal or gastric duplication cyst, may occur [59]. The extra-adrenal origin of these cysts may not be possible, but attempts to distinguish the adrenal gland from the cystic lesions with thorough US or cross-sectional imaging with MR or CT should be made.

Adrenal Abscess

Seeding of an adrenal hemorrhage in the setting of neonatal or maternal septicemia can lead to the formation of an adrenal abscess [60]. Typical organisms include *Escherichia coli,* meningococcus, group B hemolytic streptococcus, *Staphylococcus,* and *Bacteroides* [5]. On US, adrenal abscess often have a rim-like calcification, fluid filled center, echogenic debris, and increased flow and enhancement of the wall; however, the appearance is varied and may be hard to differentiate from an adrenal hemorrhage or neuroblastoma [3]. Clinical correlation of an adrenal mass in the setting of sepsis and follow-up imaging can assist with the diagnosis. Adrenal abscess complications include local extension (into the ipsilateral kidney, spleen, and pancreas), inferior vena cava compression, and rarely adrenobronchial fistula [61].

Key Points to Remember

- Given the relatively large size of the neonatal adrenal gland due to the presence of fetal adrenal cortex, ultrasound (US) can easily visualize the adrenal glands during the neonatal period.
- After the fetal cortex has involuted, ultrasound cannot reliably discern the anatomic details of the adrenal glands; therefore, computed tomography (CT) and magnetic resonance imaging (MR) are best employed for imaging the adrenal glands in children and older infants.
- On US, the normal appearance of the neonatal adrenal gland is two separate zones of echogenicity: a core consisting of a thin, central hyperechoic stripe and a surrounding rim of thicker hypoechoic tissue. The surface of a normal neonatal adrenal gland is smooth to slightly undulating, without nodular protuberances, and adrenal limbs should be uniform in length with a width of less than 4 mm.
- On CT, the adrenal gland's soft tissue attenuation is similar to the liver. On MR, on spin-echo T1-weighted images, adrenal glands have intermediate signal intensity (less than fat and similar to the liver); on T2-weighted and fat-suppressed images, adrenal glands are much brighter than fat and slightly brighter than the liver.
- Diagnosis of congenital adrenal hyperplasia can be made by the demonstration of two of three sonographic signs: (1) adrenal limb width of >4 mm, (2) cerebriform or crenated appearance of the surface of the adrenal gland, and (3) replacement of the central hyperechoic stripe with a diffusely stippled pattern of echogenicity or a diffuse thickened band of echogenicity.

- Adrenal masses in children and neonates may be attributable to hemorrhage, neoplasms, cysts, or abscesses; the age and clinical presentation of the child, in conjunction with the imaging features of the mass, will allow one to develop an appropriate list of diagnostic considerations.
- Use serial imaging to differentiate adrenal hemorrhage from neuroblastoma. Masses due to adrenal hemorrhage decrease in size over several weeks as the hemorrhage liquefies and resorbs and become more hypoechoic or anechoic, whereas in contrast, the size of a neuroblastoma is unlikely to decrease.
- Neuroblastoma has varied appearance on US, CT, and MR. Cross-sectional imaging for staging of neuroblastoma is needed in order to assess the organ of origin, extent of the tumor, local invasion, vascular encasement or displacement, calcification, lymphadenopathy, and metastases.
- Compared to adult tumors, pediatric adrenal adenoma and adrenal carcinoma are difficult to distinguish histopathologically or radiologically. Only the detection of metastases can distinguish malignant tumors from benign lesions.

Acknowledgement Ellen C. Benya, MD, Department of Medical Imaging, Ann and Robert H. Lurie Children's Hospital of Chicago for her assistance with radiological images

References

1. Daneman A, Navarro O, Haller JO. The adrenal and retroperitoneum. In: Solvis TL, editor. Caffey's pediatric diagnostic imaging. Maryland Heights: Mosby; 2007.
2. Parnaby CN, Galbraith N, O'Dwyer PJ. Experience in identifying the venous drainage of the adrenal gland during laparoscopic adrenalectomy. Clin Anat. 2008;71(7):660–5.
3. Siegel MJ, Chung EM. Adrenal glands, pancreas, and other retroperitoneal strictures. In: Siegel MJ, editor. Pediatric sonography. Philadelphia: Lippincott Williams & Wilkins; 2011.
4. Kutikov A, Crispen PL, Uzzo RG. Pathophysiology, evaluation, and medical management of adrenal disorder. In: Wein AJ, Kavoussi LR, Novick AC, Partin AW, Peters CA, editors. Campbell-Walsh urology. 10th ed. Philadelphia: Elsevier Inc; 2011.
5. Daneman A, Traubici J. The adrenal gland. In: Solvis TL, editor. Caffey's pediatric diagnostic imaging. Maryland Heights: Mosby; 2007.
6. Mitty HA. Embryology, anatomy, and anomalies of the adrenal gland. Semin Roentgenol. 1988;23(4): 271–9.
7. Barwick TD, Malhotra A, Webb JA, Savage MO, Reznek RH. Embryology of the adrenal glands and its relevance to diagnostic imaging. Clin Radiol. 2005;60(9):953–9.
8. Kempná P, Flück CE. Adrenal gland development and defects. Best Pract Res Clin Endocrinol Metab. 2008;22(1):77–93.
9. Oppenheimer DA, Carroll BA, Yousem S. Sonography of the normal neonatal adrenal gland. Radiology. 1983;146(1):157–60.
10. Kangarloo H, Diament MJ, Gold RH, Barrett C, Lippe B, Geffner M, Boechat MI, Dietrich RB, Amundson GM. Sonography of adrenal glands in neonates and children: changes in appearance with age. J Clin Ultrasound. 1986;14(1):43–7.
11. Siegel MJ, Coley B. The core curriculum: pediatric imaging. Philadelphia: Lippincott Williams & Wilkins; 2005.
12. Daneman D, Daneman A. Diagnostic imaging of the thyroid and adrenal glands in childhood. Endocrinol Metab Clin North Am. 2005;34(3):745–68.
13. Hoffman CK, Filly RA, Callen PW. The "lying down" adrenal sign: a sonographic indicator of renal agenesis or ectopia in fetuses and neonates. J Ultrasound Med. 1992;11(10):533–6.
14. Burton EM, Strange ME, Edmonds DB. Sonography of the circumrenal and horseshoe adrenal gland in the newborn. Pediatr Radiol. 1993;23(5):362–4.
15. Çakir ED, Mutlu FS, Eren E, Paşa AO, Sağlam H, Tarim O. Testicular adrenal rest tumors in patients with congenital adrenal hyperplasia. J Clin Res Pediatr Endocrinol. 2013;4(2):94–100.
16. Merke DP, Bornstein SR. Congenital adrenal hyperplasia. Lancet. 2005;365(9477):2125–36.
17. Sivit CJ, Hung W, Taylor GA, Catena LM, Brown-Jones C, Kushner DC. Sonography in neonatal congenital adrenal hyperplasia. AJR Am J Roentgenol. 1991;156(1):141–3.
18. Al-Alwan I, Navarro O, Daneman D, Daneman A. Clinical utility of adrenal ultrasonography in the diagnosis of congenital adrenal hyperplasia. J Pediatr. 1999;135(1):71–5.
19. Avni EF, Rypens F, Smet MH, Galetty E. Sonographic demonstration of congenital adrenal hyperplasia in the neonate: the cerebriform pattern. Pediatr Radiol. 1993;23(2):88–90.
20. Bentsen D, Schwartz DS, Carpenter TO. Sonography of congenital adrenal hyperplasia due to partial deficiency of 3β-hydroxysteroid dehydrogenase: a case report. Pediatr Radiol. 1997;27(7):594–5.
21. Kohda E, Yamazaki H, Hisazumi H, Tutumi Y, Ogata T, Shiraga N. Imaging of congenital lipoid adrenal hyperplasia. Radiat Med. 2006;24(3):217–19.

22. Pivonello R, De Martino MC, De Leo M, Lombardi G, Colao A. Cushing's syndrome. Endocrinol Metab Clin North Am. 2008;37(1):135–49.
23. Young Jr WF, Klee GG. Primary aldosteronism. Diagnostic evaluation. Endocrinol Metab Clin North Am. 1988;17(2):367–95.
24. Agrons GA, Lonergan GJ, Dickey GE, Perez-Monte JE. Adrenocortical neoplasms in children: radiologic-pathologic correlation. Radiographics. 1999;19(4): 989–1008.
25. Doppman JL, Travis WD, Nieman L, Miller DL, Chrousos GP, Gomez MT, Cutler Jr GB, Loriaux DL, Norton JA. Cushing syndrome due to primary pigmented nodular adrenocortical disease: findings at CT and MR imaging. Radiology. 1989;172(2):415–20.
26. Dutton RV. Wolman's disease. Ultrasound and CT diagnosis. Pediatr Radiol. 1985;15(2):144–6.
27. Ozmen MN, Aygün N, Kiliç L, Kuran L, Yalçin B, Besim A. Wolman's disease: ultrasonographic and computed tomographic findings. Pediatr Radiol. 1992;22(7):541–2.
28. Balassy C, Navarro OM, Daneman A. Adrenal masses in children. Radiol Clin North Am. 2011;49(4): 711–27.
29. Abdu AT, Kriss VM, Bada HS, Reynolds EW. Adrenal hemorrhage in a newborn. Am J Perinat. 2009;26(8):553–7.
30. Swischuk LE. Genitourinary tract and adrenal glands. In: Swischuk LE, editor. Imaging of the newborn, infant, and young child. Philadelphia: Lippincott Williams & Wilkins; 2004.
31. Heij HA, Taets van Amerongen AH, Ekkelkamp S, Vos A. Diagnosis and management of neonatal adrenal hemorrhage. Pediatr Radiol. 1989;19(6–7):391–4.
32. Mittelstaedt CA, Volberg FM, Merten DF, Brill PW. The sonographic diagnosis of neonatal adrenal hemorrhage. Radiology. 1979;131(2):453–7.
33. Miele V, Galluzzo M, Patti G, Mazzoni G, Calisti A, Valenti M. Scrotal hematoma due to neonatal adrenal hemorrhage: the value of ultrasonography in avoiding unnecessary surgery. Pediatr Radiol. 1997;27(8):672–4.
34. Calisti A, Oriolo L, Molle P, Miele V, Spagnol L. Neonatal adrenal masses: do we have reliable criteria for differential diagnosis and expectant management? Minerva Pediatr. 2012;64(3):313–18.
35. Eo H, Kim JH, Jang KM, Yoo SY, Lim GY, Kim MJ, Kim OH. Comparison of clinic-radiological features between congenital cystic neuroblastoma and neonatal adrenal hemorrhagic pseudocyst. Korean J Radiol. 2011;12(1):52–8.
36. Bergami G, Malena S, Di Mario M, Fariello G. Echography in the follow-up of neonatal adrenal hemorrhage. The presentation of fourteen cases. Radiol Med. 1990;79(5):474–8.
37. Curtis MR, Mooney DP, Vacarro TJ, Williams JC, Cendrom M, Shorter NA, Sargent SK. Prenatal ultrasound characterization of the suprarenal mas: the distinction between neuroblastoma and subdiaphragmatic extralobar pulmonary sequestration. J Ultrasound Med. 1997;16(2):75–83.
38. Franko J, Bell K, Pezzi CM. Intraabdominal pulmonary sequestration. Curr Surg. 2006;63(1):35–8.
39. Lonergan GJ, Schwab CM, Suarez ES, Carlson CL. Neuroblastoma, ganglioneuroblastoma, ganglioneuroma: radiologic-pathologic correlation. Radiographics. 2002;22(4):911–34.
40. Abramson SJ. Adrenal neoplasms in children. Radiol Clin North Am. 1997;35(6):1415–53.
41. Brodeur GM, Hogarty MD, Mosse YP, Maris JM. Neuroblastoma. In: Pizzo PA, Poplack DG, editors. Principles and practice of pediatric oncology. Philadelphia: Lippincott Williams & Wilkins; 2011.
42. Williams CM, Greer M. Homovanillic acid and vanillylmandelic acid in diagnosis of neuroblastoma. JAMA. 1963;183:836–40.
43. Cooney DR, Voorhess ML, Fisher JE, Brecher M, Karp MP, Jewett TC. Vasoactive intestinal peptide producing neuroblastoma. J Pediatr Surg. 1982;17(6): 821–5.
44. Rothenberg AB, Berdon WE, D'Angio GJ, Yamashiro DJ, Cowles RA. The association between neuroblastoma and opsoclonus-myoclonus syndrome: a historical review. Pediatr Radiol. 2009; 39(7):723–6.
45. Brodeur GM, Pritchard J, Berthold F, Carlsen NL, Castel V, Castelberry RP, De Bernardi B, Evans AE, Favrot M, Hedborg F, Kaneko M, Kemshead J, Lampert F, Lee REJ, Look AT, Pearson ADJ, Philip T, Roald B, Sawada T, Seeger RC, Tsuchida Y, Voute PA. Revisions of the international criteria for neuroblastoma diagnosis, staging, and response to treatment. J Clin Oncol. 1993;11(8):1466–77.
46. Brisse HJ, McCarville MB, Granata C, Krug KB, Wootton-Gorges SL, Kanegawa K, Giammarile F, Schmidt M, Shulkin BL, Matthay KK, Lewington VJ, Sarnacki S, Hero B, Kaneko M, London WB, Pearson AD, Cohn SL, Monclair T. Guidelines for imaging and staging of neuroblastic tumors: consensus report from the International Neuroblastoma Risk Group Project. Radiology. 2011;261(1):243–57.
47. Stark DD, Moss AA, Brasch RC, de Lorimier AA, Albin AR, London DA, Gooding CA. Neuroblastoma: diagnostic imaging and staging. Radiology. 1983; 148(1):101–5.
48. McHugh K. Renal and adrenal tumors in children. Cancer Imaging. 2007;7:41–51.
49. Sharp SE, Gelfand MJ, Shulkin BL. Pediatrics: diagnosis of neuroblastoma. Semin Nucl Med. 2011;41(5):345–53.
50. Sharp SE, Shulkin BL, Gelfand M, Salisbury S, Furman WL. 123I-MIBG scintigraphy and 18-F-FDG PET in neuroblastoma. J Nucl Med. 2009;50(8):1237–43.
51. Piccardo A, Lopa E, Conte M, Garaventa A, Foppiani L, Altrinetti V, Nanni C, Bianchi P, Cistaro A, Sorrentino S, Cabria M, Pession A, Puntoni M, Villavecchia G, Fanti S. Comparison of 18F-dopa

PET/CT and 123I-MIBG scintigraphy in stage 3 and 4 neuroblastoma: a pilot study. Eur J Nucl Mol Imaging. 2012;39:57–71.
52. Ribeiro RC, Figueiredo B. Childhood adrenocortical tumors. Eur J Cancer. 2004;40(8):1117–26.
53. Lack EE, Mulvihill JJ, Travis WD, Kozakewich HP. Adrenal cortical neoplasms in the pediatric and adolescent age group. Clinicopathological study of 30 cases with emphasis on epidemiological and prognostic factors. Pathol Annu. 1992;27(Pt 1):1–53.
54. Jimenez-Heffernan JA, Hardisson D, Palacios J, Garcia-Viera M, Gamallo C, Nistal M. Adrenal gland leiomyoma in a child with acquired immunodeficiency syndrome. Pediatr Pathol Lab Med. 1995;15(6):923–6.
55. Lin J, Wasco MJ, Korobkin M, Doherty G, Giordano TJ. Leiomyoma of the adrenal gland presenting as a non-functioning adrenal incidentaloma: case report and review of the literature. Endocr Pathol. 2007;18(4):239–43.
56. Ammoury RF, Heptulla RA, Tatevian N, Elenberg E. Laparoscopic adrenalectomy of an adrenal adenoma with myelolipoma relieves severe hypertension in a 16-year-old patient. Pediatr Nephrol. 2006;21(3):433–6.
57. Guo YK, Yang ZG, Li Y, Deng YP, Ma ES, Min PQ, Zhang XC. Uncommon adrenal masses: CT and MRI features with histopathologic correlation. Eur J Radiol. 2007;62(3):359–70.
58. Ciftci AO, Salman AB, Tanyel FC, Hiçsönmez A. Bilateral multiple adrenal pseudoocysts associated with incomplete Beckwith-Wiedemann syndrome. J Pediatr Surg. 1997;32(9):1388–90.
59. Reichelt O, Grieser T, Wunderlich H, Möller A, Schubert J. Bronchogenic cyst. A rare differential diagnosis of retroperitoneal tumors. Urol Int. 2000;64(4):216–19.
60. Steffens J, Zaubitzer T, Kirsch W, Humke U. Neonatal adrenal abscesses. Eur Urol. 1997;31(3):347–9.
61. Pointe HD, Osika E, Montagne JP, Prudent M, Tournier G, Sebbouh D. Adrenobronchial fistula complicating a neonatal adrenal abscess: treatment by percutaneous aspiration and antibiotics. Pediatr Radiol. 1997;27(2):184–5.